3838 *Chem. Mater.* **2009,** *21,* 3838–3847
DOI:10.1021/cm901381p

CHEMISTRY OF MATERIALS
Article

Self-Assembled Columnar Structures of Swallow-Shaped Tetrathiafulvalene-Based Molecules

Lei Wang,[†,∥] Soo-Jin Park,[†,∥] Se-Hyun Lee,[†] Young-Jin Kim,[†] Yun-Bae Kook,[†] Shiao-Wei Kuo,[‡] Ryan M. Van Horn,[§] Stephen Z. D. Cheng,[§] Myong-Hoon Lee,*[,†] and Kwang-Un Jeong*[,†]

[†]*Polymer Materials Fusion Research Center and Department of Polymer-Nano Science and Technology, Chonbuk National University, Jeonju 561-756, Korea,* [‡]*Department of Materials Science and Optoelectronic Engineering, National Sun Yat-Sen University, Kaohsiung 804, Taiwan, and* [§]*Maurice Morton Institute and Department of Polymer Science, The University of Akron, Akron, Ohio 44325-3909.* [∥]*These authors contributed equally to this work*

Received May 20, 2009. Revised Manuscript Received July 6, 2009

A series of swallow-shaped tetrathiafulvalene (TTF)-based liquid crystal (LC) molecules (a-6TTF*n*, where 6 represents the number of carbon atoms in the two tails of a-6TTF*n* and *n* is the even number of carbon atoms in the alkyl chains attached to the side of the asymmetric TTF mesogen, $n = 6-12$) was designed and synthesized. One of this series of swallow-shaped asymmetric TTF molecules (abbreviated as a-6TTF12) having 12 carbon atoms in the alkyl chains attached to the side of the asymmetric TTF mesogen served as an example in this study. Major phase transitions and their origins in a-6TTF12 were studied with combined techniques of differential scanning calorimetry (DSC), one-dimensional (1D) wide-angle X-ray diffraction (WAXD) and solid-state carbon-13 (^{13}C) nuclear magnetic resonance (NMR) experiments. a-6TTF12 formed a highly ordered liquid crystalline (Φ_{LC}) phase at higher temperatures and a crystalline (Φ_{Cr}) phase at lower temperatures. On the basis of the experimental results, it was found that the highly organized columns in the Φ_{LC} phase partially lost their long-range positional order compared with the Φ_{Cr} phase at lower temperatures due to the distinct molecular packing of alkyl chains during the transition from $\Phi_{LC} \leftrightarrow \Phi_{Cr}$. Furthermore, it was realized that there are two main driving forces in the formation of the ordered columnar phases. One was the $\pi-\pi$ interaction among the TTF-based mesogens, and the other was the nanophase separation between the rigid TTF-based mesogens and the flexible alkyl chains. The structure, molecular packing symmetry, and morphology of a-6TTF12 in different phases were identified using 2D WAXD together with selected area electron diffraction (SAED) from transmission electron microscopy (TEM). Bright-field TEM images of polyethylene-decorated films of a-6TTF12 allow us to confirm its molecular self-organization which was first identified by SAED as well as by 2D WAXD from oriented films. Morphological observations utilizing cross-polarized optical microscopy (POM) on the micrometer length scale validated the phase transitions and molecular orientation in the macroscopically oriented film.

Introduction

Discotic liquid crystal (LC) materials have been studied extensively as promising organic semiconductor candidates in optoelectronic devices.[1−5] The supramolecular self-assembly of discotic liquid crystals, which is generally driven by a molecular recognition process through $\pi-\pi$ interaction, plays a very important role in practical applications. It is well-known that electrical-/photoconductivity can be significantly enhanced along the long axis of self-assembled columns due to the intermolecular π-orbital overlapping between discotic building blocks.[6,7] Additionally, self-organization of LC molecules allows us to control the alignment of mesomorphic states of discotic columnar phases by applying additional external forces and allows for the minimization of defects, such as grain boundaries, which are inevitable drawbacks for charge transportation in crystalline materials.[8−11] On the basis of these reasons,

*To whom correspondence should be addressed. E-mail: kujeong@chonbuk.ac.kr (K.-U.J.) and mhlee2@chonbuk.ac.kr (M.-H.L.).

(1) Adam, D.; Schuhmacher, P.; Simmerer, J.; Haussling, L.; Siemensmeyer, K.; Etzbach, K.; Ringsdorf, H.; Haarer, D. *Nature* **1994**, *371*, 141.
(2) Craats, A. M.; Warman, J. M.; Fechtenkötter, A.; Brand, J. D.; Harbison, M. A.; Müllen, K. *Adv. Mater.* **1999**, *11*, 1469.
(3) Schmidt-Mende, L.; Fechtenkotter, A.; Müllen, K.; Moons, E.; Friend, R. H.; MacKenzie, J. D. *Science* **2001**, *293*, 1119.
(4) Gunther, H.; Emma, C.; Joaquin, B.; Berta, G.-L.; Robert, E. H.; Mara, T.; Attilio, G.; Jose, L. S. *Chem. Mater.* **2007**, *19*, 6068.
(5) Xu, Y.; Leng, S.; Xue, C.; Sun, R.; Pan, J.; Ford, J.; Jin, S. *Angew. Chem., Int. Ed.* **2007**, *46*, 3896.
(6) Sergeyev, S.; Pisulab, W.; Henri Geerts, Y. *Chem. Soc. Rev.* **2007**, *36*, 1902.
(7) Kastler, M.; Pisula, W.; Laquai, F.; Kumar, A.; Davies, R. J.; Baluschev, S.; Garcia-Gutiérrez, M.-C.; Wasserfallen, D.; Butt, H.-J.; Riekel, C.; Wegner, G.; Müllen, K. *Adv. Mater.* **2006**, *18*, 2255.
(8) Zimmermann, S.; Wendorff, J. H.; Weder, C. *Chem. Mater.* **2002**, *14*, 2218.
(9) Yoshio, M.; Kagata, T.; Hoshino, K.; Mukai, T.; Ohno, H.; Kato, T. *J. Am. Chem. Soc.* **2006**, *128*, 5570.
(10) Woon, K. L.; Aldred, M. P.; Vlachos, P.; Mehl, G. H.; Stirner, T.; Kelly, S. M.; O'Neill, M. *Chem. Mater.* **2006**, *18*, 2311.
(11) Funahashi, M.; Zhang, F.; Tamaoki, N. *Adv. Mater.* **2007**, *19*, 353.

 Published on Web 08/03/2009

various columnar LC materials including perylenetetracarboxylic acid diimides (PDIs)[12,13] and hexabenzocoronenes (HBCs)[4,14−16] have been introduced as promising semiconductor materials for organic thin-film transistors (OTFTs), organic light-emitting devices (OLEDs), and photovoltaic cells.

Among the various candidates of organic materials for optoelectronic applications,[17−22] tetrathiafulvalene (TTF) derivatives have been widely studied because of their electronic and structural characteristics. TTF derivatives are good electron donors that can form stable molecules with one or more unpaired electrons, and the planar shape of these molecules promotes the intermolecular $\pi-\pi$ stacking.[23] Most research regarding TTF and its derivatives has been focused on their crystalline phases. There are only a few reports of LC compounds based on TTF.[24−30] Recently, we reported the first room temperature columnar LCs based on TTF.[31] The incorporation of the ester group into the TTF skeleton enhanced the air stability of TTF derivatives, which is one of the main concerns for practical applications, as well as promoted the intermolecular $\pi-\pi$ interactions, leading to a favorable supramolecular self-assembly. Previous electrochemical studies of TTF derivatives indicate that they can be a *p*-type semiconductor for organic optoelectronics. However, in order to build the structure−property relationships and to improve the physical properties of TTF derivatives, it is essential to control the structure and morphology on different length scales since their physical properties strongly depend on the nature of molecular self-assembly and organization.

In order to study the nature of molecular self-assembly and organization of TTF-based molecules, we have chosen one from this series of swallow-shaped asymmetric TTF molecules (abbreviated as a-6TTF12) having 12 carbon atoms in the alkyl chains attached to the side of the asymmetric TTF mesogen. This molecule is a good example of the a-6TTF*n* series reported in ref 31, where 6 represents the number of carbon atoms in the two tails of a-6TTF*n* and *n* is the even number of carbon atoms in the alkyl chains attached to the side of the mesogen. Major phase transitions and their origins in a-6TTF12 were studied by combined techniques of differential scanning calorimetry (DSC), one-dimensional (1D) wide-angle X-ray diffraction (WAXD), and solid-state carbon-13 (^{13}C) nuclear magnetic resonance (NMR) experiments. The structures, molecular packing symmetry, and morphology in different phases were identified using 2D WAXD from oriented films and also were supported by selected area electron diffractions (SAED) from transmission electron microscopy (TEM). Bright-field TEM images of a polyethylene-decorated film of a-6TTF12 allow us to confirm its molecular self-organization which was first identified by SAED in a single domain as well as by 2D WAXD from an oriented film. Furthermore, morphological studies under cross-polarized optical microscopy (POM) supported the identification of phase transitions and molecular orientations in the macroscopically oriented film.

Experimental Section

Materials and Sample Preparation. A series of swallow-shaped TTF-based LC molecules was designed and synthesized.[31] This series of TTF derivatives was purified by column chromatography several times before examination. Their chemical structure and purity were confirmed by ^{1}H and ^{13}C NMR, Fourier-transform infrared spectroscopy (FT-IR), elemental analyses, and high-resolution mass spectrometry. One of this series of swallow-shaped asymmetric TTF molecules, a-6TTF12, was analyzed as a representative sample of the series. The chemical structure of a-6TTF12 is shown in Figure 1a. The molecular weight of a-6TTF12 was 843 g/mol. The molecular dimensions and minimal energy geometry of a-6TTF12 in the isolated gas phase were estimated by utilizing Cerius^2 (version 4.6) computer simulation software from Accelrys. The results are represented in Figure 1c−e: front (*xy*-plane), side (*yz*-plane), and top view (*xz*-plane), respectively. The calculated core length of a-6TTF12 along the *y*-axis is 1.32 nm, while the width of the core along the *x*-axis is 1.79 nm, as shown in Figure 1d and e. Assuming an all-trans conformation in the alkyl chains, the length of a-6TTF12 is 2.15 nm along the *y*-axis, and its width is 4.56 nm along the *x*-axis. It is worth noting that the TTF core and two hexyl tails at the end are in the same plane (*xy*-plane) which is perpendicular to the *xz*-plane that contains a benzoic acid ester group with a dodecyloxy alkyl tail.

(12) Struijk, C. W.; Sieval, A. B.; Dakhorst, J. E. J.; Dijk, M.; Kimkes, P.; Koehorst, R. B. M.; Donker, H.; Schaafsma, T. J.; Picken, S. J.; Craats, A. M.; Warman, J. M.; Zuilhof, H.; Sudholter, E. J. R. *J. Am. Chem. Soc.* **2000**, *122*, 11057.
(13) Würthner, F.; Chen, Z.; Dehm, V.; Stepanenko, V. *Chem. Commun.* **2006**, 1188.
(14) Craats, A. M.; Stutzmann, N.; Bunk, O.; Nielsen, M. M.; Watson, M.; Müllen, K.; Chanzy, H. D.; Sirringhaus, H.; Friend, R. H. *Adv. Mater.* **2003**, *15*, 495.
(15) Alameddine, B.; Aebischer, O. F.; Amrein, W.; Donnio, B.; Deschenaux, R.; Guillon, D.; Savary, C.; Scanu, D.; Scheidegger, O.; Jenny, T. A. *Chem. Mater.* **2005**, *17*, 4798.
(16) Pisula, W.; Menon, A.; Stepputat, M.; Lieberwirth, I.; Kolb, U.; Tracz, A.; Sirringhaus, H.; Pakula, T.; Müllen, K. *Adv. Mater.* **2005**, *17*, 684.
(17) Andrieeux, A.; Duromre, C.; Jérome, D.; Bechgaard, K. *J. Phys., Lett.* **1979**, *40*, 381.
(18) Lyskawa, J.; Le Derf, F.; Levillain, E.; Mazari, M.; Salle, M.; Dubois, L.; Viel, P.; Bureau, C.; Palacin, S. *J. Am. Chem. Soc.* **2004**, *126*, 12194.
(19) Wang, L.; Zhang, B.; Zhang, J. *Inorg. Chem.* **2006**, *45*, 6860.
(20) Mas-Torrent, M.; Rovira, C. *Chem. Commun.* **2006**, *16*, 433.
(21) Martín,, N.; Sánchez,, L.; Herranz,, M. A.; Illescas,, B.; Guldi,, D. M. *Acc. Chem. Res.* **2007**, *40*, 1015.
(22) Mas-Torrent, M.; Hadley, P.; Bromley, S. T.; Ribas, X.; Tarres, J.; Mas, M.; Molins, E.; Veciana, J.; Rovira, C. *J. Am. Chem. Soc.* **2004**, *126*, 8546.
(23) Segura, J. L.; Martín, N. *Angew. Chem., Int. Ed.* **2001**, *40*, 1372.
(24) Asahi, H.; Inabe, T. *Chem. Mater.* **1994**, *4*, 666.
(25) Bissell, R. A.; Boden, N.; Bushby, R. J.; Fishwick, C. W. G.; Holland, E.; Movaghar, B.; Bushby, R. J.; Ungar, G. *Chem. Commun.* **1998**, 113.
(26) Andreu, R.; Garín, J.; Orduna, J.; Barberá, J.; Serrano, J. L.; Sierra, T.; Sallé, M.; Gorgues, A. *Tetrahedron* **1998**, *54*, 3895.
(27) González, A.; Segura, J. L.; Martín, N. *Tetrahedron Lett.* **2000**, *41*, 3083.
(28) Gregg, B. A.; Chen, S.-G.; Cormier, R. A. *Chem. Mater.* **2004**, *16*, 4586.
(29) Katsuhara, M.; Aoyagi, I.; Nakajima, H.; Mori, T.; Kambayashi, T.; Ofuji, M.; Takanishi, Y.; Ishikawa, K.; Takezoe, H.; Hosono, H. *Synth. Met.* **2005**, *149*, 219.
(30) Pintre, I. C.; Serrano, J. L.; Ros, M. B.; Ortega, J.; Alonso, I.; Martínez-Perdiguero, J.; Folcia, C. L.; Etxebarria, J.; Goc, F.; Amabilino, D. B.; Puigmartí-Luis, J.; Gomar-Nadal, E. *Chem. Commun.* **2008**, 2523.
(31) Wang, L.; Jeong, K.-U.; Lee, M.-H. *J. Mater. Chem.* **2008**, *18*, 2657.

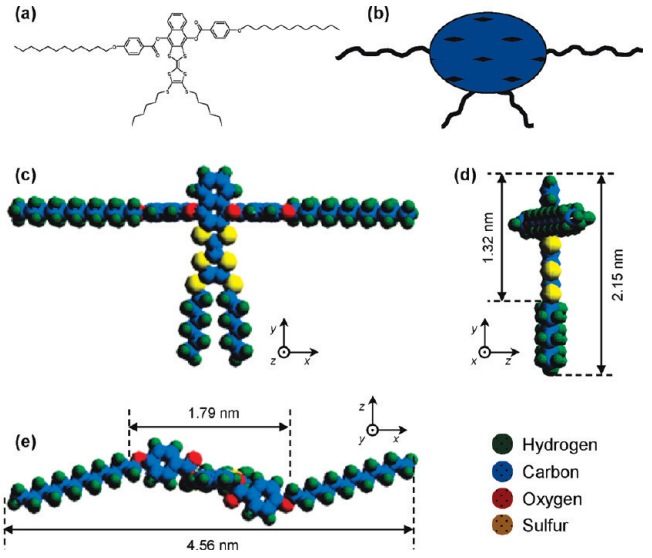

Figure 1. Chemical structure (a) and schematic illustration (b) of investigated a-6TTF12 molecule. Calculated geometric dimensions of a-6TTF12 molecule in the views from the *z*-axis (c), *x*-axis (d), and *y*-axis (e), respectively.

For one-dimensional (1D) wide-angle X-ray diffraction (WAXD) measurements, film samples with a thickness of about 1 mm were prepared by melting the a-6TTF12 compound on an aluminum plate. In order to determine the phase structures of a-6TTF12, oriented samples for 2D WAXD experiments were obtained by mechanical shearing in the LC phase and thermally treated at different temperatures. A typical sample thickness was about 0.2 mm. The samples prepared for POM had a typical thickness of 10 μm, and they were melt-processed between two bare cover glass slides. Powder samples were used for solid-state ^{13}C NMR. Thin film samples prepared for TEM via solution casting from a 0.05% (w/v) chloroform solution onto carbon-coated mica had a thickness of 50−150 nm. After evaporation of the solvent, the carbon films were floated on a water surface and recovered using TEM copper grids. In order to improve the contrast of the TEM image, Pd shadowing was applied before observation.

Equipment and Experiment. The thermal behavior of the phase transitions was studied using a Perkin-Elmer PYRIS Diamond differential scanning calorimeter (DSC) with an Intracooler 2P apparatus. The temperatures and heat flows were calibrated using material standards at cooling and heating rates ranging from 2.5 to 40 °C/min. Heating experiments always preceded the cooling experiments in order to eliminate previous thermal histories, and the cooling and heating rates were always kept identical. The transition temperatures were determined by measuring the onset temperatures from both the cooling and heating scans at different rates.

1D WAXD experiments were conducted in the reflection mode of a Rigaku 12 kW rotating-anode X-ray (Cu Kα radiation) generator coupled to a diffractometer. The diffraction peak positions and widths were calibrated with silicon crystals in the high 2θ-angle region (> 15°), and silver behenate, in the low 2θ-angle region. A hot stage was coupled to the diffractometer in order to study the structural evolutions with temperature changes during heating and cooling. The temperature of this hot stage was calibrated to be within ±1 °C error. Samples were scanned across a 2θ-angle range of 1.5−35° at a scanning rate of 2.5°/min. The oriented 2D WAXD patterns were obtained using a Rigaku X-ray imaging system with an 18 kW rotating anode X-ray generator. Silicon crystal powder, used as an internal reference, shows a diffraction ring at a 2θ value of 28.466°. A hot stage was also used to obtain diffraction peaks from the ordered structures at elevated temperatures. A 30 min exposure time was required for a high-quality pattern. In both 1D and 2D WAXD experiments, background scattering was subtracted from the sample scans.

The conformations of the alkyl chain in a-6TTF12 at different temperatures were also studied using solid-state ^{13}C NMR spectroscopy (Chemagnetics CMX 200) operating at 201.13 and 50.78 MHz for ^{1}H and ^{13}C nuclei, respectively. The samples were spun in nitrogen gas at 4.5 kHz at the magic angle. The magic angle was optimized by the intensity calibration of the aromatic carbon resonance of hexamethylbenzene. The ^{13}C cross-polarization/magic angle spinning/dipolar decoupling (CP/MAS/DD) NMR spectra were acquired to selectively investigate the rigid components, and the Bloch decay spectra with MAS/DD was used to selectively study the mobile components. The CP contact time was 1 ms, while the recycle time of the pulse was 5 s. Each spectrum consisted of an accumulation of 500 scans. The temperature of the solid-state ^{13}C NMR experiment was controlled using a REX-F900 VT unit covering the temperature range from −40 to 130 °C.

Bright-field TEM images (FEI Tecnai 12) were obtained to examine film morphology on the nanometer length scale using an accelerating voltage of 120 kV. The camera length for selected area electron diffraction (SAED) was set at 3.0 m, and the calibration of the SAED spacing smaller than 0.384 nm was carried out using evaporated thallous chloride, which has a largest first-order spacing diffraction of 0.384 nm. Spacing values larger than 0.384 nm were calibrated by doubling the *d*-spacing values of the first-order diffractions. Furthermore, the polyethylene (PE) surface lamellar decoration (SLD) technique was applied in order to study the surface topology of the self-assembled structure of a-6TTF12 in the thin films.[32−37] The decoration was conducted using linear PE as a decoration material in a vacuum evaporator. The PE was degraded, evaporated, and deposited onto the surface of the self-assembled a-6TTF12 columns.

Optical textures of the ordered phases at different temperatures were observed with cross-polarized optical microscopy (POM, Nikon ECLIPSE E600POL) coupled with a LINKAM LTS 350 heating stage in order to investigate morphology on the micrometer scale. A tint retardation plate (530 nm) was also placed between the objective lenses and the eyepieces in order to identify the orientation of molecules in the POM textures.

The Cerius^2 (version 4.6) simulation software from Accelrys was used to calculate the global equilibrium conformation of the a-6TTF12 compound in the isolated gas phase utilizing the COMPASS force field. Overlapped carbon peaks in solid-state ^{13}C NMR were resolved using the PeakFit peak separation program from Jandel Scientific. Lorentzian functions were used to obtain the best reasonable fit.

(32) Wittmann, J.-C.; Lotz, B. *Makromol. Chim. Rapid Comm.* **1982**, *3*, 733.
(33) Wittmann, J.-C.; Lotz, B. *J. Polym. Sci. Polym. Phys. Ed.* **1985**, *23*, 205.
(34) Chen, J.; Cheng, S. Z. D.; Wu, S. S.; Lotz, B.; Wittmann, J.-C. *J. Polym. Sci., Polym. Phys. Ed.* **1995**, *33*, 1851.
(35) Ge, J. J.; Xue, G.; Li, C. Y.; Man, I. K.; Zhou, W. W.; Wang, S.-Y.; Harris, F. W.; Cheng, S. Z. D.; Hong, S.-C.; Zhuang, X.-W.; Shen, Y. R. *J. Am. Chem. Soc.* **2001**, *123*, 5768.
(36) Jeong, K.-U.; Jing, A. J.; Mansdorf, B.; Graham, M. J.; Tu, Y. F.; Harris, F. W.; Cheng, S. Z. D. *Chin. J. Polym. Sci.* **2007**, *25*, 57.
(37) Jeong, K.-U.; Jing, A. J.; Monsdorf, B.; Graham, M. J.; Harris, F. W.; Cheng, S. Z. D. *J. Phys. Chem. B* **2007**, *110*, 767.

Results and Discussion

Thermal Transitions and Their Corresponding Structural Evolutions. DSC experiments were first conducted during cooling and subsequent heating at 2.5−40 °C/min scanning rates in order to detect various thermal transitions of the a-6TTF12 compound and to obtain quantitative thermodynamic properties of the thermal transitions. Figure 2a represents two exothermic thermal transitions in a set of DSC thermal diagrams during the cooling process at different cooling rates from 2.5 to 40 °C/min. The high temperature transition appears at 111 °C with a heat of transition of 31 J/g (26.1 kJ/mol) that is independent of the cooling rate. Although the width of the transition peak is broadened with the increased cooling rate, the independence of the exothermic transition temperature and its heat of transition indicate that the high temperature transition takes place close to thermodynamic equilibrium. It is worth noting that the independence of the exothermic transition temperature and its heat of transition are often observed from an isotropic melt (I) to a liquid crystal (Φ_{LC}) phase.[38−51] On the other hand, the onset temperature and the heat of transition of the low temperature exothermic transition shifts to lower temperatures with an increase in the cooling rate. At a cooling rate of 2.5 °C/min, the onset temperature of the low temperature exothermic transition is 10 °C and its heat of transition is 25 J/g (21.1 kJ/mol). However, the onset temperature and heat of transition at 40 °C/min are 8 °C and 16 J/g (13.5 kJ/mol), respectively. This cooling rate dependence of the transition usually implies a crystallization process.[38−51]

Figure 2b shows the subsequent heating diagrams immediately following the cooling process at different scanning rates. There are two endothermic transitions,

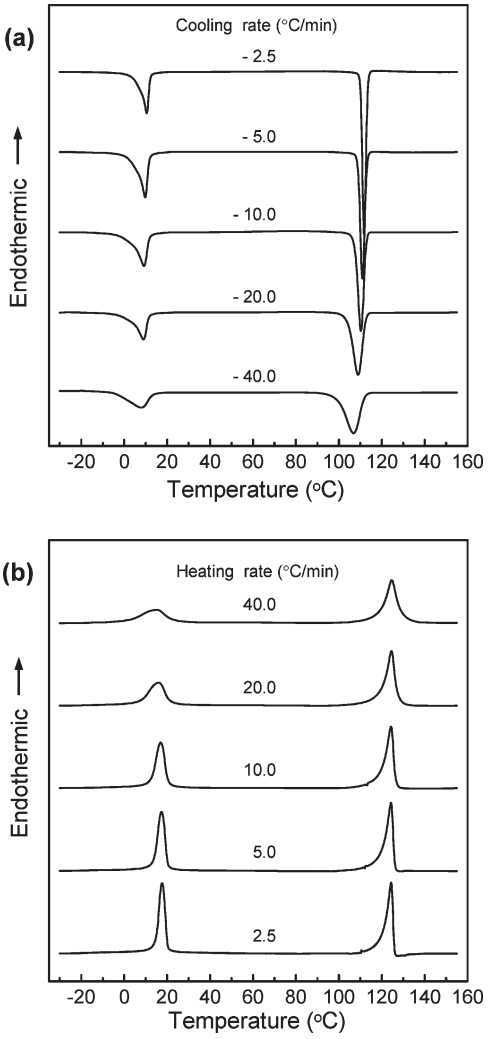

Figure 2. Sets of DSC cooling (a) and subsequent heating (b) thermal diagrams for a-6TTF12 at scanning rates ranging from 2.5 to 40 °C/min.

which correspond to the two exothermic transitions found during the previous cooling process. The high temperature transition is the I ↔ Φ_{LC} transition, again, supported by the independence of its transition temperature and heat of transition on heating rates, while the low-temperature transition must be crystal melting. The thermodynamic parameters from the subsequent heating process correspond well with those from the previous cooling process. The possible molecular origins of these thermal transitions need to be identified via solid-state ^{13}C NMR (represented in the Supporting Information) and WAXD experiments at different temperatures.

Although DSC experiments are sensitive to heat absorption and release events at thermal transitions and can give quantitative thermodynamic properties, this technique does not usually provide direct information regarding what types of ordered structures are associated with the transitions. Therefore, structure sensitive techniques such as 1D WAXD experiments need to be conducted at different temperatures to identify the corresponding structural evolutions of a-6TTF12. Figure 3 shows a set of 1D WAXD patterns obtained by cooling the a-6TTF12 compound from 150 to −10 °C at a cooling

(38) Ungar, G.; Feijoo, J. L.; Percec, V.; Yourd, R. *Macromolecules* **1991**, *24*, 953.
(39) Yandrasits, A.; Cheng, S. Z. D.; Zhang, A.; Cheng, J.; Wunderlich, B.; Percec, V. *Macromolecules* **1992**, *25*, 2112.
(40) Pardey, R.; Zhang, A.; Gabori, P. A.; Harris, F. W.; Cheng, S. Z. D.; Adduci, J.; Facinelli, J. V.; Lenz, R. W. *Macromolecules* **1992**, *25*, 5060.
(41) Pardey, R.; Shen, D.; Gabori, P. A.; Harris, F. W.; Cheng, S. Z. D.; Adduci, J.; Facinelli, J. V.; Lenz, R. W. *Macromolecules* **1993**, *26*, 3687.
(42) Yoon, Y.; Zhang, A.; Ho, R.-M.; Cheng, S. Z. D.; Percec, V.; Chu, P. *Macromolecules* **1996**, *29*, 294.
(43) Yoon, Y.; Ho, R.-M.; Moon, B.; Kim, D.; McCreight, K. W.; Li, F.; Harris, F. W.; Cheng, S. Z. D.; Percec, V.; Chu, P. *Macromolecules* **1996**, *29*, 3421.
(44) Zheng, R.-Q.; Chen, E.-Q.; Cheng, S. Z. D.; Xie, F.; Yan, D.; He, T.; Percec, V.; Chu, P.; Ungar, G. *Macromolecules* **1999**, *32*, 3574.
(45) Zheng, R.-Q.; Chen, E.-Q.; Cheng, S. Z. D.; Xie, F.; Yan, D.; He, T.; Percec, V.; Chu, P.; Ungar, G. *Macromolecules* **1999**, *32*, 6981.
(46) Jeong, K.-U.; Jin, S.; Ge, J. J.; Knapp, B. S.; Graham, M. J.; Ruan, J.; Guo, M.; Xiong, H.; Harris, F. W.; Cheng, S. Z. D. *Chem. Mater.* **2005**, *17*, 2852.
(47) Jeong, K.-U.; Knapp, B. S.; Ge, J. J.; Jin, S.; Graham, M. J.; Xiong, H.; Harris, F. W.; Cheng, S. Z. D. *Macromolecules* **2005**, *38*, 8333.
(48) Jeong, K.-U.; Knapp, B. S.; Ge, J. J.; Jin, S.; Graham, M. J.; Harris, F. W.; Cheng, S. Z. D. *Chem. Mater.* **2006**, *18*, 680.
(49) Jeong, K.-U.; Knapp, B. S.; Ge, J. J.; Graham, M. J.; Tu, Y.; Leng, S.; Xiong, H.; Harris, F. W.; Cheng, S. Z. D. *Polymer* **2006**, *47*, 3351.
(50) Jeong, K.-U.; Yang, D. K.; Graham, M. J.; Tu, Y.; Kuo, S. W.; Knapp, B. S.; Harris, F. W.; Cheng, S. Z. D. *Adv. Mater.* **2006**, *18*, 3229.
(51) Yang, D.-K.; Jeong, K.-U.; Cheng, S. Z. D. *J. Phys. Chem. B* **2008**, *112*, 1358.

rate of 2.5 °C/min. There are two phase transitions observed in the 1D WAXD patterns, which agree well with the observations in the DSC cooling diagrams (Figure 2a). At temperatures above 111 °C, a-6TTF12 is in the I phase exhibiting only two amorphous halos at $2\theta = 4.20°$ (d-spacing = 2.10 nm) and $2\theta = 20.33°$ (d-spacing = 0.44 nm), which correspond to the average periodicity of electron density fluctuations between the nanophase-separated TTF cores and alkyl tails and to the average distance among the amorphous chains, respectively. When the temperature reached 110 °C during cooling, which corresponds to the high temperature thermal transition observed using DSC (Figure 2a and b), many sharp reflection peaks suddenly appeared in both the low- and wide-angle regions. It is not certain whether this phase is defined as a crystalline phase or a highly ordered LC phase. However, based on the previous DSC experiments of which the high temperature thermodynamic properties do not depend on the cooling and subsequent heating rate, this transition should be close to the thermodynamic equilibrium, as discussed previously, that occurs for the phase transitions from the I phase to a mesophase, such as LC phases.[38−51] In this case, nevertheless, even if this phase is a mesophase, it must possess some highly ordered molecular structure since sharp diffractions exist in the wide-angle region. Note that for the low-ordered nematic (N), smectic A (SmA), and smectic C (SmC) LC phases, sharp reflections only appear in the small-angle region in WAXD. A possible ordered scheme may be that the rigid mesogens are packed in an ordered fashion, yet the flexible alkyl chains are in disordered states, similar to many previous reports.[5,52−58] This speculation must be supported by spectroscopic experiments, such as solid-state ^{13}C NMR (represented in the Supporting Information), at different temperatures to detect the conformational and molecular mobility changes of the rigid aromatic mesogens and the flexible alkyl chains at the transitions.

Below the low temperature thermal transition, a structural change is obvious as shown in Figure 3 of the 1D WAXD results. The number of Bragg reflections significantly decreased by decreasing the temperature below 10 °C, and a broad amorphous halo appeared around $2\theta = 27°$ (d-spacing = 0.33 nm). This 1D WAXD result indicates that the highly ordered mesophase structure between 111 and 10 °C has rapidly changed when the temperature passed through this low temperature thermal transition. The structural order of the TTF-based mesogens in the a-6TTF12 compound now needs to accommodate the crystallization of the alkyl chains during the low temperature thermal transition. This is different from conventional LC materials during their crystallizations.[48,59,60]

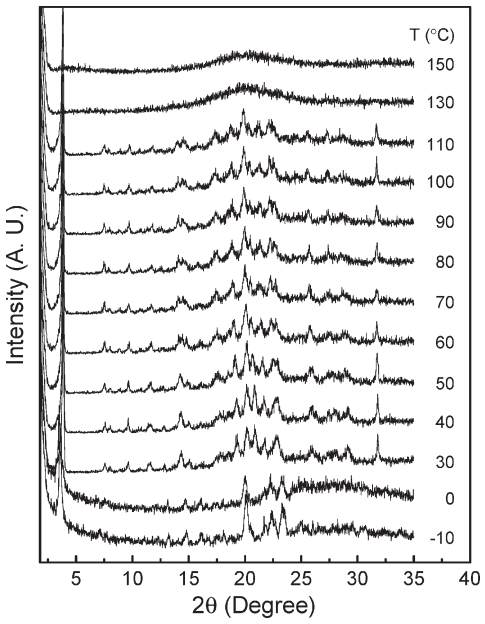

Figure 3. Set of 1D WAXD powder patterns of a-6TTF12 during cooling at a rate of 2.5 °C/min at different temperatures between 150 and −10 °C.

On the basis of both the DSC and 1D WAXD results, it is evident that the a-6TTF12 compound forms two ordered phases below the isotropic phase. In particular, we speculated that the phase at low temperature is a result of the compensation between the higher-ordered mesogens and the crystallization of the alkyl tails. In order to support this speculation and to know the molecular origin of these structural transitions, solid-state ^{13}C NMR experiments of a-6TTF12 at different temperatures with both CP/MAS/DD (Figure S2) and Bloch decay (Figure S3) methods have been conducted and are shown in the Supporting Information. These solid-state ^{13}C NMR experiments provided information on the fraction of ordered (all-trans) and disordered (mixture of trans and gauche) conformations in the alkyl chains and the mobility of each carbon in a-6TTF12 in different phases at various temperatures.[61−65] These results show that the alkyl chains are frozen in the amorphous state after the high temperature transition and are nearly crystalline (90% trans conformation) at the low temperature transition. By combination of DSC (Figure 2), 1D

(52) El-ghayoury, A.; Douce, L.; Skoulios, A.; Ziessel, R. *Angew. Chem., Int. Ed.* **1998**, *37*, 1255.
(53) Struijk, C. W.; Sieval, A. B.; Dakhorst, J. E. J.; van Dijk, M.; Kimkes, P.; Koehorst, R. B. M.; Donker, H.; Schaafsma, T. J.; Picken, S. J.; van de Craats, A. M.; Warman, J. M.; Zuilhof, H.; Sudhölter, E. J. R. *J. Am. Chem. Soc.* **2000**, *122*, 11057.
(54) Mori, A.; Yokoo, M.; Hashimoto, M.; Ujiie, S.; Diele, S.; Baumeister, U.; Tschierske, C. *J. Am. Chem. Soc.* **2003**, *125*, 6620.
(55) Carbonnier, B.; Andreopoulou, A. K.; Pakula, T.; Kallitis, J. K. *Macromol. Chem. Phys.* **2005**, *206*, 66.
(56) Riala, P.; Andreopoulou, A.; Kallitsis, J.; Gitsas, A.; Floudas, G. *Polymer* **2006**, *47*, 7241.
(57) Prehm, M.; Liu, F.; Zeng, X.; Ungar, G.; Tschierske, C. *J. Am. Chem. Soc.* **2008**, *130*, 14922.
(58) Lehmann, M.; Jahr, M.; Grozema, F. C.; Abellon, R. D.; Siebbeles, L. D. A.; Müller, M. Adv. Mater. **2008**, *20*, ASAP.
(59) Kouwer, P. H. J.; Swager, T. M. *J. Am. Chem. Soc.* **2007**, *129*, 14042.
(60) Yang, G.-Z.; Wang, W.-Z.; Wang, M.; Liu, T. *J. Phys. Chem. B* **2007**, *111*, 7747.
(61) Cheng, J.; Jin, Y.; Wunderlich, B.; Cheng, S. Z. D.; Yandrasits, M. A.; Zhang, A.; Percec, V. *Macromolecules* **1992**, *25*, 5991.
(62) Cheng, J.; Yoon, Y.; Ho, R.-M.; Leland, M.; Guo, M.; Cheng, S. Z. D.; Chu, P.; Percec, V. *Macromolecules* **1997**, *30*, 4688.
(63) Ge, J. J.; Guo, M.; Zhang, Z.; Honigfort, P. S.; Mann, I. K.; Wang, S. Y.; Harris, F. W.; Cheng, S. Z. D. *Macromolecules* **2000**, *33*, 3983.
(64) McElheny, D.; Grinshtein, J.; Frydman, V.; Frydman, L. *Macromolecules* **2002**, *35*, 3544.
(65) Ishida, H.; Horii, F. *Macromolecules* **2002**, *35*, 5550.

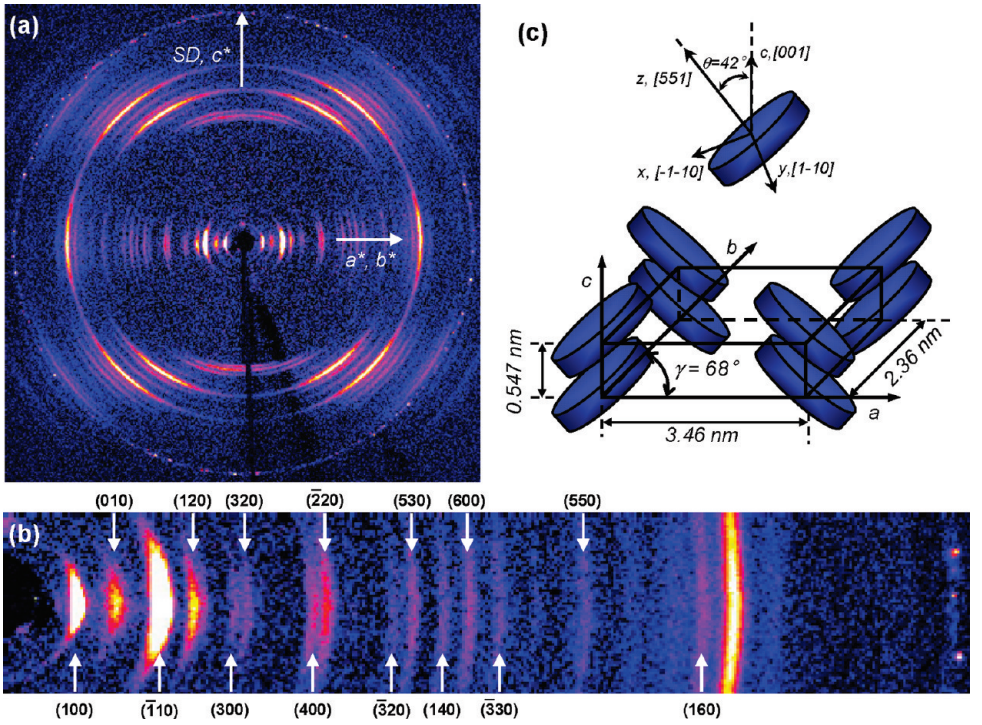

Figure 4. (a) 2D WAXD pattern of the highly ordered columnar Φ_{LC} phase of a-6TTF12 at room temperature. (b) Assignment of equatorial reflections between $2\theta = 2.5°$ and $2\theta = 17.5°$ based on the 2D a^*b^* lattice. (c) Schematic unit model with a-6TTF12 for the highly ordered columnar phase of a-6TTF12.

WAXD (Figure 3), and solid-state ^{13}C NMR (Figures S2 and S3 in the Supporting Information) results, it can be concluded that a-6TTF12 exhibited two ordered phases below T_i. The high temperature phase transition is induced by the organization of TTF-based rigid mesogens, which creates the highly ordered LC phase. In this highly ordered LC phase, alkyl tails at the end and the sides of the TTF-based mesogen are in the isotropic melt state, while the TTF-based mesogens are in a highly ordered solid state. The alkyl chain crystallization at the low temperature transition forced the reorganization of TTF-based mesogens. The last statement is clearly supported by Bragg reflections in 1D WAXD (Figure 3).

Structural Identification and Morphological Observations. None of the DSC, solid-state ^{13}C NMR or 1D WAXD techniques provide direct information about the structural symmetry changes at the transitions. In order to obtain detailed structural and symmetry information in each of these two phases, 2D WAXD experiments from oriented samples and SAED experiments from an ordered, single structural domain must be conducted.

Figure 4a shows a 2D WAXD pattern of an oriented a-6TTF12 sample at 30 °C. The sample was prepared by mechanical shearing just below the high temperature transition and subsequently quenched to room temperature. The incident X-ray beam direction is normal to the shear direction (the SD along the meridian). This 2D WAXD pattern exhibits diffractions on the equator and meridian as well as in the quadrants, indicating that this phase possesses a 3D-ordered phase. However, the fact that alkyl tails in a-6TTF12 at room temperature are in the liquid state, which is indicated by the solid-state ^{13}C NMR experimental results, should be taken into account. Furthermore, the diffraction pairs along the meridian and in the quadrants possess broader arcs compared with those along the equator. This may reveal that the structure is a pseudo-3D-ordered structure.

As shown in Figure 4a, the a^* and b^* axes are assigned to the equator, while the c^*-axis is parallel to the meridian direction (SD). On the equator in the low 2θ-angle region in Figure 4a and b, there are three diffractions close to the X-ray beam stop at 2.55, 3.74, and 5.26° corresponding to d-spacings of 3.46, 2.36, and 1.67 nm, respectively. On the basis of the triangulation method of building a 2D a^*b^* lattice of the unit cell,[66] these three diffractions on the equator can be assigned to be the (100), (010), and ($\bar{1}$10) diffractions accordingly. A series of relatively weak diffractions on the equator between $2\theta = 5.5°$ and 22° fit well with the 2D a^*b^* lattice, and they can be assigned as shown in Figure 4c. Through the refinement of the reciprocal 2D a^*b^* lattice using the diffractions on the equator, a real space 2D unit cell is calculated with dimensions of $a = 3.46$ nm, $b = 2.36$ nm, and $\gamma = 68°$.

A pair of relatively diffuse diffraction arcs at $2\theta = 16.2°$ (d-spacing = 0.547 nm) is observed on the meridian (along the c^*-axis), as shown in Figure 4a. This pair of diffuse diffraction arcs can be identified as the (001) plane. This assignment is also supported by a series of diffractions of the first layer ($hk1$) of the 2D WAXD pattern. Because the (001) diffraction is on the meridian

(66) Eashoo, M.; Wu, Z.; Zhang, A.; Shen, D.; Tse, C.; Harris, F. W.; Cheng, S. Z. D.; Gardner, K. H.; Hsiao, B. S. *Macromol. Chem. Phys.* **1994**, *195*, 2207.

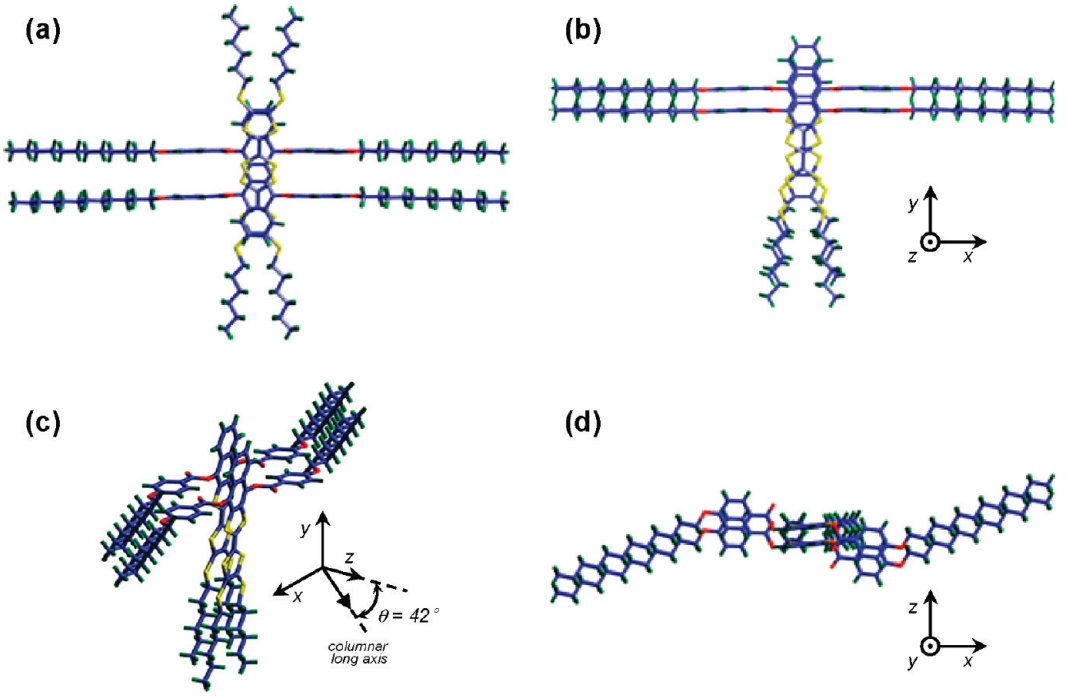

Figure 5. Two proposed computer-generated, energy-minimized packing models of Φ_{LC} phase: view of antiparallel (AB packing) mode (a) and views of parallel (AA packing) mode from different viewing angles (b−d).

with $2\theta = 16.2°$ and the a^* and b^* axes are along the equator, the dimension of c is 0.547 nm, and the angles of α and β are 90°. Careful structural analysis gives a pseudo-3D monoclinic unit cell with dimensions of $a = 3.46$ nm, $b = 2.36$ nm, $c = 0.547$ nm, $\alpha = \beta = 90°$, and $\gamma = 68°$ via the refinement of the reciprocal lattice. This phase can thus be identified as a highly ordered columnar LC phase, and it is abbreviated as the Φ_{LC} phase. The experimentally observed and the calculated 2θ values and d-spacings based on this unit cell lattice are listed in Table 1. Its calculated crystallographic density is 0.99 g/cm^3 based on one a-6TTF12 molecule per unit cell. The experimentally observed density is 0.98 g/cm^3, which fits well with the calculated data.

Among the (hkl) diffractions in the quadrants, the diffraction at $2\theta = 24.6°$ (d-spacing = 0.362 nm) is especially interesting. This diffraction may be assigned as the (551) diffraction, which is located ~48° away from the equator, and it should be representative of the $\pi-\pi$ interaction of TTF-based mesogens. Therefore, this diffraction can be interpreted as TTF-based mesogen columns along the shear direction (SD, c^*-axis), and they are synclinically tilted within the column ~42° away from the long axis of the columns. Owing to the requirement of 2D columnar close packing, the tilting direction of adjacent neighboring columns should be tilted in the opposite direction of the adjacent one. This argument can be supported by diffractions in all four quadrants. A schematic illustration representing the unit cell lattice and the columnar molecular packing of the Φ_{LC} phase of a-6TTF12 is shown in Figure 4c.

A remaining question is: how do a-6TTF12 molecules pack into a column with the 42° tilting away from the column axis? In order to find an answer for this question, the minimum energy geometry of a-6TTF12 in the isolated gas phase was first obtained by utilizing Cerius[2] (version 4.6) computer simulation software from Accelrys. Energy minimization of a-6TTF12 at the absolute zero temperature is performed under the COMPASS force field. As described in the Experimental Section, the TTF rigid core and two hexyl tails at the end of the TTF core are on the same plane (xy-plane) which is perpendicular to the plane (xz-plane) containing a benzoic acid ester group with a dodecyloxy alkyl tail (Figure 1).

Table 1. Experimental and Calculated Crystallographic Parameters of the Highly-Ordered Liquid Crystalline (Φ_{LC}) Phase of a-6TTF12

	2θ (deg)		d-spacing (nm)	
hkl	expt[a]	calc[b]	expt[a]	calc[b]
010	3.74	3.74	2.36	2.36
100	2.55	2.55	3.46	3.46
$\bar{1}10$	5.25	5.26	1.68	1.67
120	6.95	6.95	1.26	1.27
140	14.2	14.3	0.62	0.62
160	21.7	21.8	0.41	0.40
200	5.10	5.10	1.73	1.72
$\bar{2}20$	10.5	10.5	0.84	0.83
300	7.66	7.66	1.15	1.14
320	8.48	8.48	1.04	1.04
$\bar{3}20$	12.6	12.6	0.70	0.70
$\bar{3}30$	15.7	15.8	0.56	0.56
400	10.2	10.2	0.86	0.87
530	13.5	13.5	0.66	0.65
550	18.4	18.4	0.48	0.48
001	16.2	16.2	0.55	0.55
011	16.6	16.6	0.53	0.53
101	16.4	16.4	0.54	0.54
$\bar{1}11$	17.0	17.1	0.52	0.52
201	17.0	17.0	0.52	0.52
551	24.6	24.6	0.36	0.36

[a] The accuracy of the experimental data is ± 0.005 nm. [b] The calculated data listed are based on the highly ordered liquid crystalline (Φ_{LC}) monoclinic unit cell with $a = 3.46$ nm, $b = 2.36$ nm, $c = 0.55$ nm, $\alpha = \beta = 90.0°$, and $\gamma = 68°$.

Because these two planes are arranged perpendicular to each other, there are only two most probable molecular packings. One is an antiparallel molecular arrangement (AB packing), and the other is a face-to-face parallel molecular packing (AA packing), which are illustrated in Figure 5a and b−d, respectively. In this case, we assume that the minimized energy geometry of a-6TTF12 in the isolated gas phase is frozen and that they are close enough to interact. In the case of the face-to-face parallel molecular packing (Figure 5b−d), both planes in the minimized energy geometry of a-6TTF12 approach 0.36 nm to maximize the $\pi-\pi$ interactions between aromatic moieties, while the planes containing benzoic acid ester groups with a dodecyloxy alkyl tail are at 0.52 nm, which is not close enough to create the $\pi-\pi$ interactions in the AB packing model (Figure 5a). On the basis of this simple computer calculation, it is assumed that the molecular packing sequence of a-6TTF12 in a column must be the AA packing, as shown in Figure 5b−d.

This structural determination and the existence of columns in the Φ_{LC} phase of a-6TTF12 can also be supported by TEM morphology and SAED pattern experiments. Figure 6a shows a bright-field image of the morphology of the highly ordered columnar Φ_{LC} phase of a-6TTF12 at room temperature. The existence of columns in this morphology is confirmed by the SAED pattern as shown in Figure 6b. The SAED pattern is obtained from the circled area in Figure 6a without sample tilting. A pair of strong electron diffraction spots appears at a *d*-spacing of 2.36 nm, which is close to the (010) X-ray diffraction of the 2D WAXD pattern (Figure 4a and b). Even its second- and third-order diffraction can be clearly seen at *d*-spacings of 1.18 and 0.79 nm, respectively. Therefore, the *b**-axis is assigned to be along the equator, and the column direction is parallel to the surface of the substrate where the column is highly ordered. The arrow in Figure 6a points to the long axis of the columns which corresponds to the *c**-axis of the Φ_{LC} unit cell. The assignment of the (001) diffraction at $2\theta = 16.2°$ (*d*-spacing = 0.547 nm) on the meridian of 2D WAXD of a-6TTF12 (Figure 4a) can be confirmed by the observation of electron diffraction spots at *d*-spacing = 0.547 nm on the meridian. Furthermore, two pairs of electron diffraction spots at *d*-spacing = 0.533 nm and at *d*-spacing = 0.496 nm belong to the (011) and (021) X-ray diffractions of the 2D WAXD pattern (Figure 4a).

In order to further support the a-6TTF12 packing model in the *bc*-plane (along the [100] zone, see Figure 6b), the PE lamellar decoration experiment was conducted on the surface of the Φ_{LC} phase.[32−37] The result is shown in Figure 7. In this figure, the PE crystal nanorods are parallel to the *b**-axis, which is perpendicular to the *c*-axis. This indicates that the chain axes of the PE oligomers recognize the column axis and thus, are deposited along the *c*-axis. This surface topological information of the Φ_{LC} phase

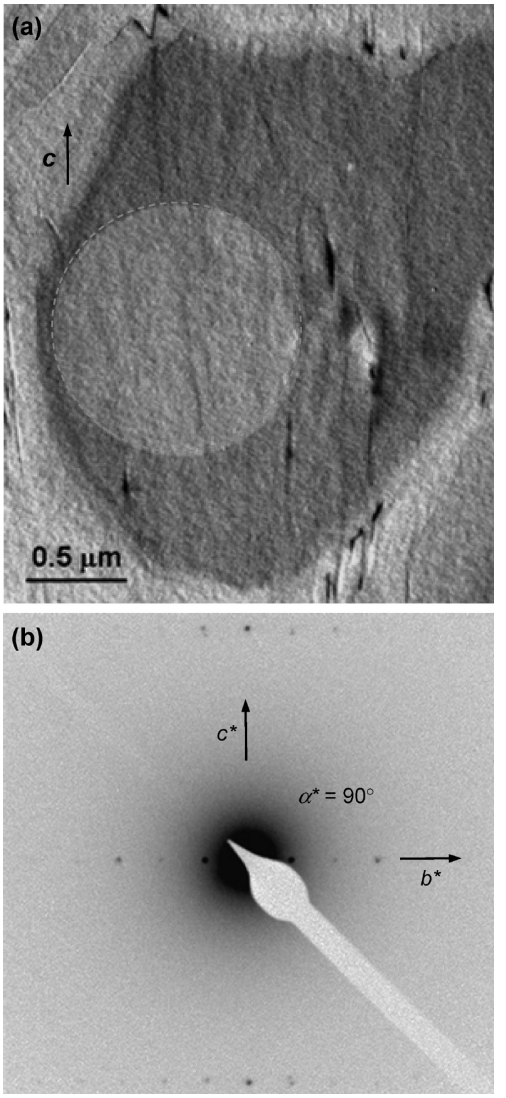

Figure 6. (a) Bright-field TEM morphology of the highly ordered columnar Φ_{LC} phase of a-6TTF12. The arrow points along the long axis of the columns (*c*- and *c**-axis). (b) SAED pattern from the circled area of the bright-field TEM morphology in part a.

agrees well with the proposed molecular packing model, similar to the results reported previously.[67,68]

The texture changes in POM give rise to morphological information on the micrometer length scale. In order to confirm the macroscopic molecular orientation of the highly ordered Φ_{LC} phase, a mechanically oriented Φ_{LC} phase film was observed utilizing POM. Figure 8a shows the POM micrograph of a-6TTF12 sheared at 110 °C and then annealed at room temperature. The bright "lines" are the oriented bulk sample, and the shear direction is along these "lines." The "lines" are bright because the molecules are in the ordered columnar Φ_{LC} phase, and the direction of refractive indices is not parallel to the directions of the polarizer or analyzer of the POM. A tint retardation plate (530 nm) was also applied between objective lenses and eyepieces in order to identify the orientation of molecules in the POM textures, as shown in

(67) Xue, C.; Jin, S.; Weng, X.; Ge, J. J.; Shen, Z.; Shen, H.; Graham, M. J.; Jeong, K.-U.; Huang, H.; Zhang, D.; Guo, M.; Harris, F. W.; Cheng, S. Z. D. *Chem. Mater.* **2004**, *16*, 1014.

(68) Jeong, K.-U.; Jing, A. J.; Mansdorf, A. B.; Graham, M. J.; Harris, F. W.; Cheng, S. Z. D. *J. Phys. Chem. B* **2007**, *110*, 767.

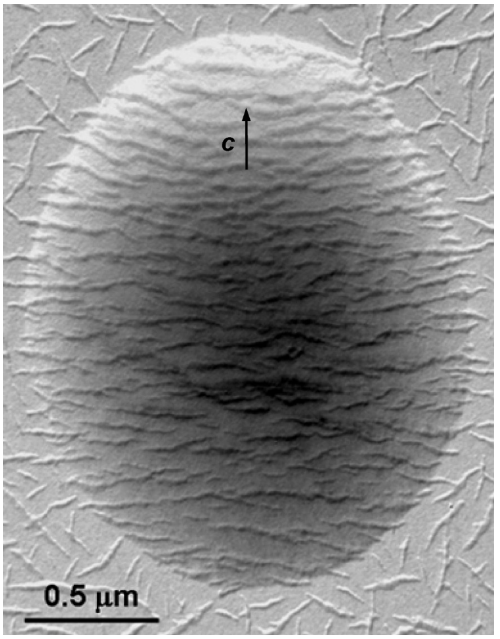

Figure 7. TEM micrograph after the PE surface lamellar decoration on the a-6TTF12 film surface.

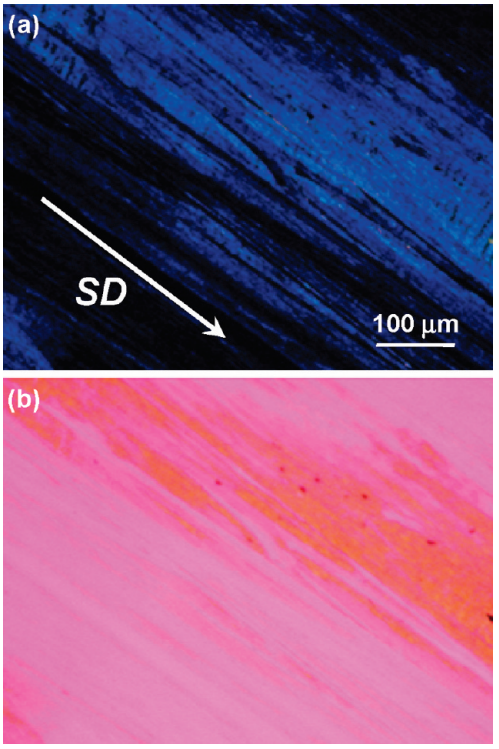

Figure 8. (a) POM morphological observation of a-6TTF12 sheared at 110 °C and then annealed at room temperature. (b) POM texture with a tint plate between the objective lenses and eyepieces.

Figure 8b. The sheared "lines" are yellow in color, which means that the refractive index perpendicular to the "lines" ($n_{\perp}$) is higher than the refractive index parallel to the "lines" ($n_{\parallel}$). Therefore, the column direction of this supramolecular columnar phase should align along the

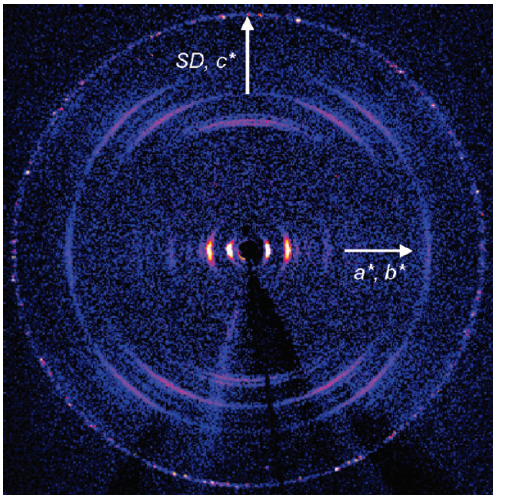

Figure 9. 2D WAXD pattern of the Φ_{Cr} phase of a-6TTF12 at 3 °C.

"lines" (shear direction, SD).[69,70] This observation is also consistent with the 2D WAXD result (Figure 4) and the SAED experiment (Figure 6b).

In the DSC at different scanning rates and 1D WAXD experiments at different temperatures, it has been realized that below 10 °C alkyl chains are crystallized and distort the order of columns. The structure determination for the Φ_{Cr} phase is also obtained via a 2D WAXD experiment. The oriented Φ_{Cr} phase was prepared by mechanical shearing at 110 °C and subsequent quenching to room temperature. Then, this oriented sample was cooled down to 3 at 2.5 °C/min. The 2D WAXD of the Φ_{Cr} phase was obtained at 3 °C. As shown in Figure 9, the 2D WAXD of the Φ_{Cr} phase is indeed different compared with that of the Φ_{LC} phase (Figure 4). As observed in previous 1D WAXD experiments, the high order of diffractions disappeared, and the *d*-spacings of the diffractions are shifted. As indicated in Figure 9, the a^* and b^* axes are along the equator and the c^*-axis is on the meridian. The molecular organization in the Φ_{Cr} phase is thus not much different from that of the Φ_{LC} phase. Careful structural analysis of the 2D WAXD pattern of the Φ_{Cr} phase gives a monoclinic unit cell with dimensions of $a = 3.72$ nm, $b = 1.79$ nm, $c = 0.54$ nm, $\alpha = \beta = 90°$, and $\gamma = 72°$ via the refinement of the reciprocal lattice.

The structural transformation from the Φ_{LC} phase to the Φ_{Cr} phase identified by the combination of DSC (Figure 2), solid-state ^{13}C NMR (Figure S2) and WAXD (Figures 3, 4, and 9) experiments can be supported by the texture changes in POM. The optical textures of a-6TTF12 upon cooling at 1 °C/min from 130 °C to −10 °C have been recorded, and textures at 30 and 5 °C are shown in Figure 10a and b, respectively. The photograph taken at 30 °C (Figure 10a) shows a typical mosaic texture often observed in the highly ordered columnar phase.[69,70] Further decreasing the temperature to 5 °C results in small but strong birefringent aggregates which must be associated with the Φ_{Cr} phase (Figure 10b).

(69) Shen, H.; Jeong, K.-U.; Xiong, H. M.; Graham, M. J.; Leng, S. W.; Zheng, J. X.; Huang, H. B.; Guo, M. M.; Harris, F. W.; Cheng, S. Z. D. *Soft Matter* **2006**, *2*, 232.

(70) Dierking, I. *Textures of Liquid Crystals*; Wiley-VCH: Weinheim, 2003.

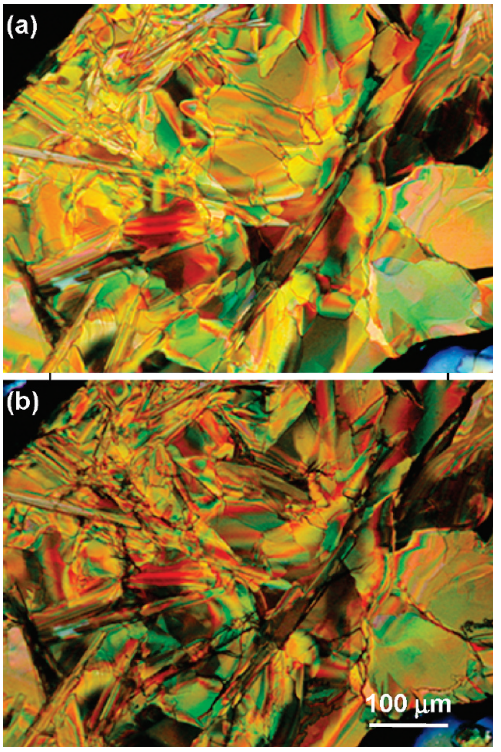

Figure 10. POM morphological observation of a-6TTF12 at 30 (a) and 5 °C (b).

Conclusion

A swallow-shaped TTF molecule (a-6TTF12) having 12 carbon atoms in the alkyl chains attached to the side of a TTF mesogen was designed and synthesized. Its molecular self-assembly was studied utilizing the combined techniques of DSC, 1D/2D WAXD, SAED, and solid-state ^{13}C NMR. On the basis of the experiments and careful analysis, it was determined that a-6TTF12 formed a highly ordered Φ_{LC} phase at higher temperatures and a Φ_{Cr} phase at lower temperatures. Furthermore, it was found that the highly organized columns in the Φ_{LC} phase partially lost their long-range positional order in the Φ_{Cr} phase at lower temperatures. The solid-state ^{13}C NMR and WAXD results combined with DSC indicate that this phenomenon is due to the molecular packing process of alkyl chains during the transition of $\Phi_{LC} \leftrightarrow \Phi_{Cr}$. It was also realized that there are two main driving forces in the formation of the ordered columnar phases. One was the $\pi-\pi$ interaction among the TTF-based mesogens, which is the main driving force of phase transition of $I \leftrightarrow \Phi_{LC}$. The other was the nanophase separation between the rigid TTF-based mesogens and the flexible alkyl chains. The structures, molecular packing symmetry, and morphology of a-6TTF12 in two ordered phases were identified using 2D WAXD together with SAED in TEM. Bright-field TEM images of a polyethylene-decorated film of a-6TTF12 provided topological evidence of column formation which was first identified by SAED as well as by 2D WAXD from the oriented film. The phase transitions and molecular orientations in the macroscopically oriented film were also studied by POM experiments. The highly ordered columnar Φ_{LC} phase of a-6TTF12 at room temperature may provide a promising candidate material for organic optoelectronic devices, which is currently under investigation.

Acknowledgment. This work was mainly supported by KRF-2008-314-D00121 (CBNU, Korea) and partially by NSF-DMR-0516602 (UA, USA). L.W. would like to acknowledge the 2008 Postdoc Program of CBNU.

Supporting Information Available: Molecular mobility in the a-6TTF12 compound studied by solid-state ^{13}C NMR. This material is available free of charge via the Internet at http://pubs.acs.org.